

Control of Water Vapor Permeation through Oxide Films on Polymers for Flexible Displays

Won Hoe Koo, Sang Hun Choi, Hong Koo Baik*, Sung Man Lee¹, and Se Jong Lee²

Department of Metallurgical Engineering, Yonsei University, Seoul 120-749, Korea

¹Department of Advanced Material Science and Engineering,

Kangwon National University, Chuncheon 200-701, Korea

²Department of Materials Engineering, Kyungshung University, Busan 608-736, Korea

Composite films consisting of tin oxide and silicon oxide produced via thermal evaporation were deposited on polycarbonate substrates as water-barrier films to control the polarizability and packing density of the composite films, both of which are factors significantly affecting water vapor permeation through the films. As the tin oxide was added to the silicon oxide, the polarizability and packing density of the composite films increased, and the water vapor transmission rate (WVTR) through the composite oxide films decreased. Because of their strong interaction with water vapor, the 80 % tin oxide films with the highest polarizability and packing density showed the lowest WVTR; however, the loose microstructures, which were caused by thermal evaporation, resulted in a WVTR still too high to be applied as passivation layers in organic light emitting diodes. Therefore, we deposited SnO₂ films with high polarizability on polycarbonate substrates while using an ion-beam-assisted deposition process (IBAD) to increase the packing density. This process resulted in a WVTR below the measurable limit of 0.01 g/m²/day at 100% RH and 37.8°C. The permeation mechanism of water vapor through the oxide films is discussed in terms of the chemical interaction with water vapor and the microstructure of the oxide films. The chemical interaction of water vapor with oxide films was investigated by the refractive index obtained from ellipsometry and the OH group peak obtained from x-ray photoelectron spectroscopy (XPS). The microstructure of the composite oxide films was characterized using atomic force microscopy (AFM) and transmission electron microscopy (TEM). The activation energy for water vapor permeation through the oxide films was also measured in relation to the permeation mechanism of water vapor.

Keywords: polarizability, packing density, ion-beam assisted deposition (IBAD), water vapor transmission rate

1. INTRODUCTION

Inorganic transparent oxide films, such as silicon- and aluminum-oxide on polymer substrates have been widely used as gas barriers in food packaging, medical devices and, more recently, flexible display industries. In particular, for passivation of organic light emitting devices (OLEDs) requiring an extremely low water-vapor transmission rate (WVTR) of $<10^{-6}$ g/m²/day at 100 % RH and 25 °C,^[1] relatively dense oxynitride films, such as AlO_xN_y and SiO_xN_y, compared to AlO_x and SiO_x, have been studied as transparent gas barrier materials with using sputtering and plasma-enhanced chemical vapor deposition (PECVD)^[2-4]. However, since these reported barrier films show too high WVTR to be applied to display industries and the permeation mechanism of water vapor has not been well known. Therefore, a new barrier mate-

rial design based on the permeation mechanism of water vapor is required to provide reliable protection against the permeation of water vapor. In addition, because all layers except for indium tin oxide in OLEDs are deposited by thermal evaporation, it would be profitable for any new barrier material to be deposited by thermal evaporation to enable a continuous process.

We investigated the material properties necessary to protect against the permeation of water vapor using composite oxide films, which consisted of silicon oxide and tin oxide and were deposited by thermal evaporation. From the experimental results, we found that the main factors affecting the permeation of water vapor through oxide films are high polarizability and high packing density. Therefore, we utilized an ion-beam-assisted-deposition (IBAD) process to protect against the permeation of water vapor reliably by densifying the oxide films with high polarizability. We then investigated the effect of the packing density and the polariz-

*Corresponding author: thinfilm@yonsei.ac.kr

ability of the oxide films on the permeation of water vapor, in terms of the microstructure and chemical interaction of the oxide films with the water vapor.

2. EXPERIMENTAL PROCEDURE

Composite films consisting of SiO_x and SnO_2 were deposited via thermal evaporation onto optical-grade polycarbonates (PC) and Si (100) wafer substrates. In addition, SiO_x and SnO_2 films were deposited via an IBAD process, using an End-Hall ion gun. The PC substrates, each with a thickness of 200 μm , have no 'antiblock' particles inducing micro-scale defects in the deposited films and a very smooth surface of the rms (surface roughness) below 1 nm. An anti-electrostatic gun was used to remove the surface electrostatic charge on the PC substrates following a cleaning with alcohol. The working pressure was first kept at 1.1×10^{-2} Pa, with an oxygen flow rate of 2 sccm during the thermal evaporation method, then at 2.67×10^{-2} Pa, with an oxygen flow rate of 1.5 sccm and argon flow rate of 3 sccm during the IBAD process. The anode voltage of the End-Hall ion gun was 150 V, and the ion beam current incident on the substrate, which was measured using a Faraday cup, varied from 10 to 45 mA/cm². The evaporation source materials were mixed oxides of SiO and SnO_2 with various atomic concentration ratios. Powders of SiO and SnO_2 , with purities of 99.99% and 99.9%, respectively, were combined in atomic concentration ratios from 5 : 1 to 1 : 2 and were evaporated on the tungsten boats. The film growth rate was maintained at 0.1 nm/s by using a quartz crystal monitor, and the films thickness was fixed at 80 nm.

The refractive index for the films deposited on the Si(100) substrates was measured at 633 nm using a L117 ellipsometer (Gaertner Scientific Corporation). The structure of the films on the PC substrates was determined by XRD (Rigaku, D/max-RINT 2700) operating at 30 kV, 20 mA, and using a Cu $K\alpha_1$ line; all the films showed amorphous structures. The surface morphology of the films on the PC substrates was examined by AFM with a Digital Instruments Nanoscope II. The AFM images of $1 \times 1 \mu\text{m}$ were obtained during tapping mode. The microstructure of the films by IBAD was observed by TEM (JEOL 2010F) operating at 200 keV. For the TEM analysis, the deposited films on PC were placed on 400-mesh copper grids, and the PC substrates were completely dissolved by the heated o-chlorophenol vapor to 120 °C. The chemical compositions and the chemical bonding states of the films were analyzed by monochromatic XPS (VG Scientific, ESCARLAB 220-IXL) using an Al $K\alpha$ X-ray with energy of 1486.6 eV and a take-off angle of 90°. Narrow scan spectra of all the regions of interest were recorded with 20 eV pass energy, and the binding energy scale was referred to the C1s peak of the carbon contaminating the sample surface at a value of 284.6 eV. From the Si2p

and Sn3d peak deconvolution, we found that the SiO_x films and the SnO_x films obtained by thermal evaporation had oxygen compositions of around 1.7 and 2, respectively, and that all the films obtained by IBAD had oxygen compositions of around 2. Water vapor transmission rate (WVTR) and activation energy for water vapor permeation was measured at 100% RH using a Permatran W 3/31 (Modern controls, Inc.). The samples were masked with aluminum foil having a 5-cm² gas exposure area for water vapor transmission, and the data were taken at temperatures ranging from 27 to 47.8 °C.

3. RESULTS AND DISCUSSION

3.1. Oxide's polarizability and chemical interaction with water vapor

Since water has a large dipole moment and lone-pair electrons, and thus is a good donor, molecular adsorption occurs by acid/base interaction between water vapor and the oxides. Therefore, strong adsorption on the internal surface of pores and the top surface of oxide films occurs easily in more basic oxides with the generation of an OH group on the surface^[5]. Since basicity of oxides, defined as the average electron donor power, is closely related to oxides' polarizability, which can be expressed as the refractive index, oxides with a higher polarizability and refractive index result in a higher OH group density on the top surface and an internal surface within pores by stronger interaction with water vapor^[6-8]. The formed OH groups within the pores may interact with permeating water vapor, interrupt the continuous permeation of water vapor and thus decreasing the water vapor transmission rate. The bond strength between OH groups and water bonded to the OH groups is so strong that desorption of water vapor bonded to OH groups begins above 150 °C^[9-10] and increases with the polarizability of oxides. Therefore, it is thought that oxide materials with a high refractive index effectively protect against the permeation of water vapor through the oxide films.

To investigate the effects of the polarizability of the oxide films on water vapor permeation, we deposited composite films consisting of SnO_2 of high refractive index and SiO_x of low refractive index by thermal evaporation. Figure 1(a) indicates that the refractive index of the composite films increases with an increasing SnO_2 content, and it shows a maximum value for the composition of 80% SnO_2 , which designates the highest polarizability. These results are consistent with the results of Feldman et al. for ZrO_2 - SiO_2 and Y_2O_3 - SiO_2 and of Koo et al. for CeO_2 - SiO_2 composite films produced by coevaporation^[11-13].

Figure 2 shows the deconvoluted O1s XPS peaks of the deposited films with SnO_2 contents of 0, 80, and 100%. The O1s peak of the SnO_2 films in Fig. 2(c) shows the peak related to the OH groups at around 531.6 eV with the O1s

peak of FWHM 1.33 eV corresponding to the Sn^{4+} at around 530.3 eV. In contrast, the O1s peak of the SiO_x films shows no peaks related to the OH groups in Fig. 2(a) except for the O1s peak with FWHM 1.63 eV for SiO_x . Because the polarizability and refractive index of SnO_2 is higher than those of SiO_x , a higher OH group density formed on the surface, and this was confirmed by the XPS results in Fig. 2. The 80% SnO_2 films with the highest refractive index show a higher OH group density than the SnO_2 films, as shown in Fig. 2 (b).

3.2. WVTR and effects of the composite film micro-structure

Figure 3 shows the WVTR measured at 37.8 °C through the composite films deposited on the PC. The pure SiO_x and SnO_2 films provide approximately 2.4 times improvement in WVTR, as compared to the bare PC substrate (34 $\text{g}/\text{m}^2/\text{day}$). As the SnO_2 content in the composite films increases, the refractive index and the OH group density increases, and the WVTR decreases, reaching the lowest value of about 1 $\text{g}/\text{m}^2/$

day at the composition of 80% SnO_2 . The deposition of the 80% SnO_2 films with the highest refractive index shows a WVTR reduction of about 34 times, which suggests that the surface OH groups within pores caused by the polarizability of the oxide films significantly affects the permeation of water vapor. In addition, the 80% SnO_2 films have more effective water vapor barrier properties than the SiO_x , AlO_x , and AlO_xN_y deposited by PECVD, electron beam evaporation, and sputtering methods^[3, 14-15]. However, although the SnO_2 films have a high refractive index of about 1.9, the water vapor transmission rate is similar to the SiO_x films with a refractive index of about 1.44. This result may be associated with the films' porosity, because if the pore size and density is too large and high, the permeating water vapor would be expected to penetrate the films with little interaction through the central pore space away from the surface OH groups within the pores or with weak interaction with multilayer of the water vapor adsorbed on the surface OH groups within pores.

Feldman et al. remarked that the unusual variations in the

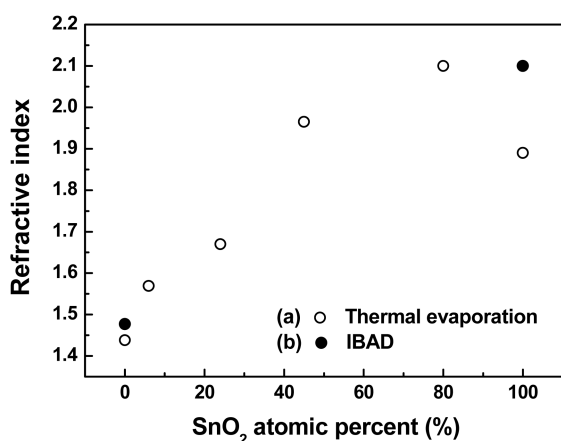


Fig. 1. Refractive index of (a) the composite films (○) by thermal evaporation with various SnO_2 atomic concentrations (0%, 6%, 45%, 80%, 100%), and (b) the SiO_x and SnO_2 films (●) produced via IBAD.

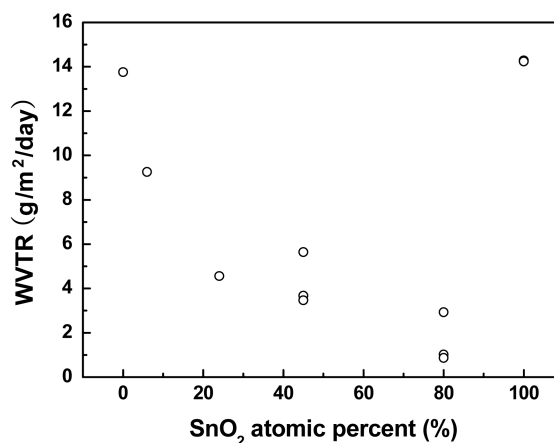


Fig. 3. Water vapor transmission rates (WVTRs) for the composite films on PC at 37.8 °C and 100% RH as a function of the atomic concentration of tin oxide.

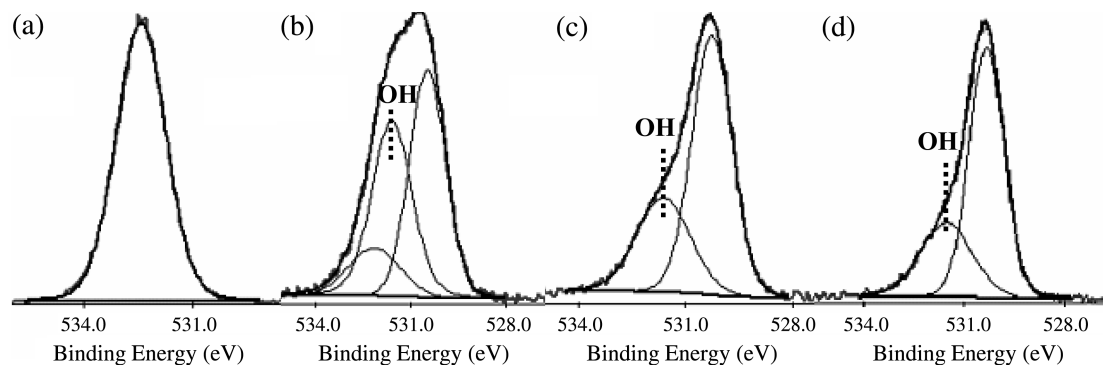


Fig. 2. The deconvoluted O1s XPS peaks of the deposited films with SnO_2 contents of (a) 0, (b) 80, (c) 100% produced via thermal evaporation, and (d) the SnO_2 films produced via IBAD. The peak at around 531.6 eV is related to the OH groups, and the 80% SnO_2 films show the highest OH group density because they have the highest polarizability.

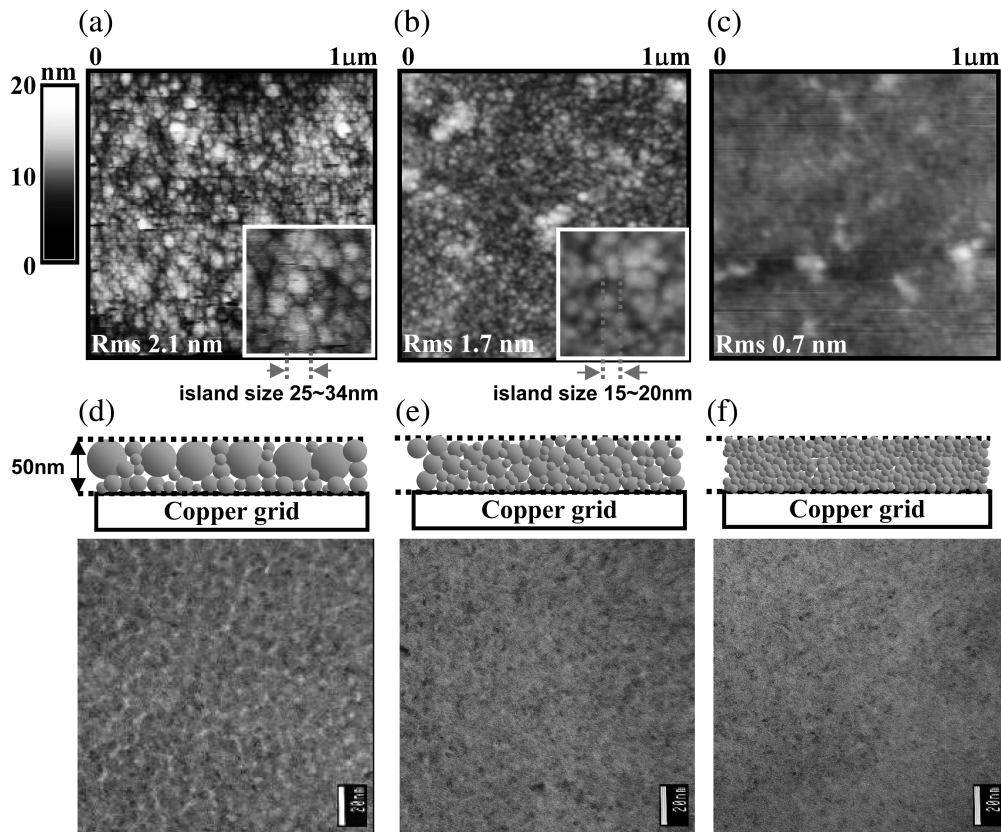


Fig. 4. The AFM images of the SnO₂ films (a) the 80% SnO₂ films, (b) coated by thermal evaporation, and (c) the SnO₂ films produced via IBAD at an ion beam current density of 45 $\mu\text{A}/\text{cm}^2$. The TEM images for each AFM image are also shown in (d), (e), and (f) with the illustrations indicating the microstructure of each film.

refractive index in ZrO₂-SiO₂ and Y₂O₃-SiO₂ originated from the densification of the composite films, because the refractive index of the films was closely related to the microstructure and the packing density^[11-12]. Therefore, the highest refractive index in the 80% SnO₂ films implies a high packing density and a dense microstructure. The densification of the 80% SnO₂ films was confirmed by the AFM and TEM images shown in Fig. 4. The SnO₂ films with a high refractive index, shown in Fig. 4 (a), show a loose structure consisting of spherical particles of large sizes, ranging from 25 to 34 nm, with a surface roughness of 2.1 nm. In contrast, the 80% SnO₂ films show a relatively a dense structure of spherical particles sized from 15 to 20 nm with an rms of 1.7 nm. The large pores between the spherical particles in the SnO₂ films as a path of water vapor permeation are indicated by the light area in the plane view images with a clear contrast shown in Fig. 4(d). However, the 80% SnO₂ films show indistinct contrast in Fig. 4(e), implying relatively small pores and densely packed particles^[16]. Therefore, the SnO₂ films, in spite of their high refractive index, show a high WVTR of 14 g/m²/day, as compared to 1 g/m²/day for the 80% SnO₂ films.

3.3. Activation energy of water vapor through the composite films

The effects of the polarizability and the packing density of the films on the permeation of water vapor can be evaluated by investigating the activation energy for water vapor permeation, which can be calculated using the following Arrhenius equation:

$$\Pi = \Pi_0 \exp(-\Delta E/RT).$$

where Π is the transmission rate, ΔE is the activation energy of permeation, R is the universal gas constant, T is absolute temperature, and Π_0 is a constant unique to the system. Figure 5 shows the water vapor transmission data measured between 27 °C and 47.8 °C, presented in Arrhenius form with the calculated activation energy from its slope. The activation energy for water vapor permeation through the thermal-evaporated SiO_x and SnO₂ films is about 9 kJ/mol and 13 kJ/mol higher, respectively, than that measured for the bare PC (40.5 kcal/mol). The activation energy of the 80% SnO₂ films is about ~41 kJ/mol higher, as compared to that for the bare PC. The increased activation energy for each film implies that the permeating water vapor interacts with the films deposited on the PC, and the different activation

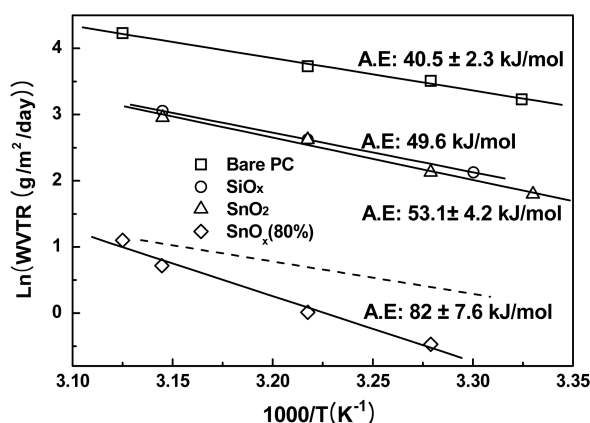


Fig. 5. Dependence of the water vapor transmission rate on reciprocal temperature for the bare PC (□), PC/SiO_x films (○), PC/SiO_x films (△), and PC/the 80% SnO₂ films (◇) produced via thermal evaporation. The dashed line corresponding to the bare PC is intended to clearly show the difference in activation energy.

energy indicates that the type and strength of the interaction with the water vapor is different according to the polarizability and film porosity of the oxides.

As mentioned above, water vapor easily adsorbs on the oxide surface, forming OH groups. Additional water vapor adsorbs on the hydroxylated surface with strong interaction, and then the continuing water vapor adsorbs on top of each other to form multi-layers by weak van der Waal's attraction force between water vapors. The strong interaction between the OH groups and water vapor increases with the polarizability of oxides¹⁷. In contrast, the weak water-water interaction is independent of the polarizability of oxides. In the films with large pores and low packing density, the water-water interaction may be dominant during the permeation of water vapor through the films, via the formation of multi-layer water vapor on the pores. If the pore size is significantly reduced, the interaction between the OH groups and the permeating water vapor may become dominant.

The similar activation energy in consideration of error range and the low additional activation energy, in the thermal-evaporated SiO_x and SnO₂ films indicates that the weak water-water interaction independent of the polarizability of the oxides influences the permeation of water vapor through the films. The 80% SnO₂ films show a higher activation energy than that of the SiO_x and SnO₂ films, because the 80% SnO₂ films with high polarizability have high OH group density and strong interaction between the OH groups and the permeating water vapor.

3.4. Water barrier properties of the oxide films produced via IBAD

Although the 80% SnO₂ films show water vapor barrier properties superior to those of the pure SiO_x and SnO₂ films, the WVTR of 1 g/m²/day is still too high value to be applied

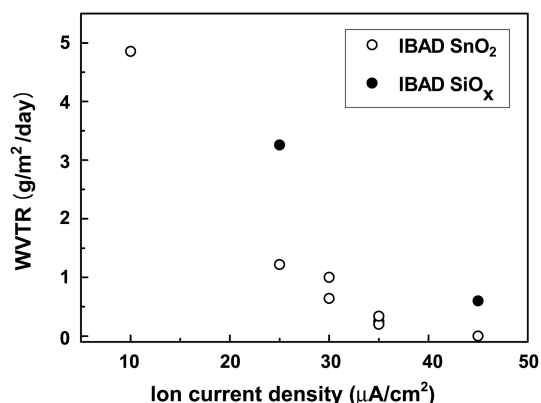


Fig. 6. Water vapor transmission rates (WVTRs) of the SiO_x films (●) and SnO₂ films (○) deposited by IBAD process as a function of the ion current density, measured at 37.8 °C and 100% RH.

as a passivation layer in flexible display industries, such as OLED and OTFT. This is because thin films deposited by thermal evaporation originally have loose microstructures due to the low adatom mobility. Therefore, we used an End-Hall ion gun to control the densification of the oxide films with high refractive index. Because the deposition of the 80% SnO₂ films increases the ambient temperature to around 70 °C and 100 °C during thermal evaporation and IBAD, respectively, we used the easily evaporated SnO₂ as an evaporation source with high refractive index during IBAD, and we attempted to limit the ambient temperature to below 85 °C.

The SnO₂ films produced via thermal evaporation show a high WVTR, due to the loose microstructure and in spite of their high refractive index, as seen in Fig. 3. Ion bombardment during the deposition in IBAD enhances the adatom mobility, and thus significantly increases the packing density of the films with an increase of refractive index. We examined the water vapor barrier properties of the SnO₂ films as varying the ion beam current density from 0 to 45 μA/cm² and compared with the SiO_x films with low refractive index.

Figure 6 shows the WVTRs of the SiO_x and SnO₂ films deposited via the IBAD process as a function of the ion beam current density, which was measured at 37.8 °C and 100 % RH. As the ion beam current density increases, the WVTR of the SiO_x and SnO₂ films on the PC substrate rapidly decreases from the WVTR of 14 g/m²/day corresponding to the SiO_x and SnO₂ films produced via thermal evaporation. The SnO₂ films show lower WVTRs than those of the SiO_x films at all ion beam current densities. At an ion beam current density of 45 μA/cm², the SnO₂ films show a WVTR below the measurable limit of 0.01 g/m²/day, while the SiO_x films show a higher WVTR of 0.6 g/m²/day. The different water barrier properties of the SiO_x films and SnO₂ films at the same ion beam current are attributed to the different reactivity with water vapor.

Ion bombardment during deposition in IBAD promotes film densification and the film densification is closely related to the refractive index, resulting in the increase of the refractive index. Thus, the SiO_x and SnO_2 films produced via IBAD at an ion beam current density of $45 \mu\text{A}/\text{cm}^2$, as shown in Fig. 1(b), show increased refractive index values of 1.48 and 2.05, respectively, as compared to the SiO_x and SnO_2 films produced via thermal evaporation. A high OH group density is generated on the surface of the SnO_2 films by IBAD, as seen in Fig. 2(d), which coincides with the results of the SnO_2 films produced via thermal evaporation, as shown in Fig. 2(c). In addition, ion bombardment induces many nucleation sites and enhanced adatom mobility, and thus the SnO_2 films produced via IBAD at an ion beam current density of $45 \mu\text{A}/\text{cm}^2$, as shown in Fig. 4(c), show densely packed structures composed of fine particles with a rms of 0.7 nm, where the pore size becomes extremely small, in contrast with the large pore size of the thermal-evaporated SnO_2 films due to large size of spherical particles in Fig. 4(a). The illustrations and TEM images in Fig. 4(f) reflect the different microstructures of the SnO_2 films by IBAD. The indiscernible contrast in the TEM image of Fig. 4(f) implies that the SnO_2 films produced via IBAD are composed of densely packed fine particles^[16]. Therefore, the continuous transfer of water vapor through the oxide films is effectively protected in the SnO_2 films densified by ion bombardment, due to the stronger interaction between the OH groups and the permeating water vapor, as well as to a higher OH group density than that of the SiO_x films.

Figure 7 shows the water vapor transmission data measured between 27°C and 47.8°C , presented in Arrhenius form, with the calculated activation energy from its slope, for the SiO_x and SnO_2 films with a WVTR of 1.58 and $0.2 \text{ g}/\text{m}^2/\text{day}$ at an ion beam current density of $35 \mu\text{A}/\text{cm}^2$. The SnO_2 films deposited at an ion beam current density of $45 \mu\text{A}/\text{cm}^2$ cannot be used because they have a WVTR below the measurable limit of $0.01 \text{ g}/\text{m}^2/\text{day}$. The activation energies of the SiO_x and SnO_2 films produced via IBAD show high values of $\sim 66 \text{ kJ}/\text{mol}$ and $\sim 104 \text{ kJ}/\text{mol}$, respectively, compared to $\sim 41 \text{ kJ}/\text{mol}$ of the bare PC. The SiO_x and SnO_2 films deposited at an ion beam current density of $35 \mu\text{A}/\text{cm}^2$ show higher activation energy than the thermal-evaporated films, indicating the influence of the strong interaction between the OH groups and the permeating water vapor, rather than the weak water-water interaction. In addition, a much higher additional energy of $\sim 63 \text{ kJ}/\text{mol}$ is needed for the permeation of water vapor through the SnO_2 films produced via IBAD, while a relatively low additional energy of $\sim 25 \text{ kJ}/\text{mol}$ is needed for the SiO_x films produced via IBAD. This is because the OH group density and the interaction strength between the OH groups and water vapor, in the films with the significantly reduced pore size by ion bombardment, increase with the polarizability of the films. P.

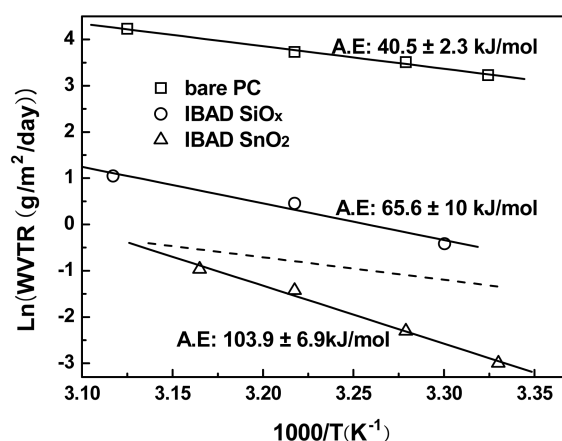


Fig. 7. Dependence of WVTR on reciprocal temperature for the bare PC (□), PC/ SiO_x films (○), and PC/ SnO_2 films produced via IBAD at an ion current density of $35 \mu\text{A}/\text{cm}^2$ (△). The dashed line corresponding to the bare PC is intended to clearly show the difference in activation energy.

Paghu, et al. measured the desorption energy of water vapor adsorbed on the OH groups for ZrO_2 , HfO_2 , and SiO_2 films^[17]. The desorption energy of water vapor adsorbed on the OH groups was 33, 27, and 19 kJ/mol, for ZrO_2 , HfO_2 , and SiO_2 films, respectively, consistent with the order of polarizability. Therefore, such a higher additional energy is needed for the water vapor permeation through the SnO_2 films deposited at the an ion beam current density of $35 \mu\text{A}/\text{cm}^2$, and when the packing density is more enhanced and the pore size is minimized by the an increased ion beam current density of $45 \mu\text{A}/\text{cm}^2$, the SnO_2 films show a WVTR below measurable limit of $0.01 \text{ g}/\text{m}^2/\text{day}$.

4. CONCLUSION

We have demonstrated that water vapor permeation through oxide films is controlled by the oxide's polarizability and the packing density of the oxide films. This is because oxide films with high polarizability and high packing density form high OH groups on the pore, induce strong interaction between the OH groups and the permeating water vapor, and thus protect against the permeation of water vapor. Therefore, densified SnO_2 films with high polarizability produced by ion bombardment show superior water barrier properties to SiO_x films with low polarizability, and they have WVTRs below the measurable limit of $0.01 \text{ g}/\text{m}^2/\text{day}$ at an ion beam current density of $45 \mu\text{A}/\text{cm}^2$.

REFERENCES

1. M. S. Weaver, L. A. Michalski, K. Rajan, M. A. Rothman, J. A. Silvernail, J. J. Brown, P. E. Burrows, G. L. Graff, M. E. Gross, P. M. Martin, M. Hall, E. Mast, C. Bonham, W. Bennett, and M. Zumhoff, *Appl. Phys. Lett.* **81**, 2929

- (2002).
2. M. Vogt and R. Hauptmann, *Surf. Coat. Technol.* **74-75**, 676 (1995).
 3. A. G. Erlat, B. M. Henry, J. J. Ingram, D. B. Mountain, A. McGuigan, R. P. Howson, C. R. M. Grovenor, G. A. D. Briggs, and Y. Tsukahara, *Thin Solid Films* **388**, 78 (2001).
 4. A. G. Erlat, B. M. Henry, J. J. Ingram, C. R. M. Grovenor, G. A. D. Briggs, R. J. Chater, and Y. Tsukahara, *J. Phys. Chem. B* **108**, 883 (2004).
 5. V. E. Henrich and P. A. Cox, *The Surface Science of Metal Oxides*, p. 255, Cambridge University Press, New York NY (1996).
 6. W. H. Koo, S. M. Jeong, S. H. Choi, H. K. Baik, S. M. Lee, and S. J. Lee, *J. Phys. Chem. B* **108**, 18884 (2004).
 7. V. Dimitrov and T. Komatsu, *J. Sol. Sta. Chem.* **163**, 100 (2003).
 8. S. Takeda M. Fukawa, Y. Hayashi, and K. Matsumoto, *Thin Solid Films* **339**, 220 (1999).
 9. A. Feng, J. McCoy, Z. A. Munir, and D. E. Cagliostro, *J. Coll. Int. Sci.* **180**, 276 (1996).
 10. N. Yamazoe, J. Fuchigami, and M. Kishikawa, *Surf. Sci.* **86**, 335 (1979).
 11. A. Feldman, E. N. Farabaugh, W. K. Haller, D. M. Sanders, and R. A. Stempniak, *J. Vac. Sci. Technol. A* **4**, 2969 (1986).
 12. A. Feldman, X. Ying, and E. N. Farabaugh, *Appl. Opt.* **28**, 5229 (1989).
 13. W. H. Koo, S. M. Jeong, S. H. Choi, H. K. Baik, S. J. Lee, and K. M. Song, *Thin Solid Films* **468**, 28 (2004).
 14. Y. G. Tropsha and N. G. Harvey, *J. Phys. Chem. B* **101**, 2259 (1997).
 15. C. S. Deng, H. E. Assender, F. Dinelli, O. V. Kolosov, G. A. D. Briggs, T. Miyamoto, and Y. Tsukahara, *J. Polym. Sci. Part B Polym. Phys.* **38**, 3151 (2000).
 16. A. G. Erlat, R. J. Spontak, R. P. Clarke, T. C. Robinson, P. D. Haaland, Y. Tropsha, N. G. Harvey, and E. A. Vogler, *J. Phys. Chem. B* **103**, 6074 (1999).
 17. P. Raghu, C. Yim, F. Shadman, and E. Shero, *AIChE. J.* **50**, 1881 (2004).